FEBS Letters

FEBS PRESS
science publishing by scientists

RESEARCH ARTICLE

Structural characterisation of a MAPR-related archaeal cytochrome b_{5M} protein

Sarah Teakel[1], Michealla Marama[2], David Aragão[3,*], Sofiya Tsimbalyuk[1], Emily R. R. Mackie[4,5], Tatiana P. Soares da Costa[4,5], Jade K. Forwood[1] and Michael A. Cahill[1,6]

1 School of Dentistry and Medical Sciences, Charles Sturt University, Wagga Wagga, Australia
2 School of Animal and Veterinary Sciences, Charles Sturt University, Wagga Wagga, Australia
3 Australian Synchrotron, Australian Nuclear Science and Technology Organisation, Clayton, Australia
4 Department of Biochemistry and Genetics, La Trobe Institute for Molecular Science, La Trobe University, Bundoora, Australia
5 School of Agriculture, Food & Wine and Waite Research Institute, University of Adelaide, Glen Osmond, Australia
6 The John Curtin School of Medical Research, The Australian National University, Canberra, Australia

Correspondence
M. A. Cahill and J. K. Forwood, School of Dentistry and Medical Sciences, Charles Sturt University, Wagga Wagga, NSW 2678, Australia
Tel: +612 6933 2317
E-mail: mcahill@csu.edu.au (MAC); jforwood@csu.edu.au (JKF)

Present address
*Diamond Light Source, Harwell Science and Innovation Campus, Didcot, UK

(Received 13 June 2022, revised 27 July 2022, accepted 28 July 2022, available online 22 August 2022)

doi:10.1002/1873-3468.14471

Edited by Peter Brzezinski

We recently reported that the membrane-associated progesterone receptor (MAPR) protein family (mammalian members: PGRMC1, PGRMC2, NEUFC and NENF) originated from a new class of prokaryotic cytochrome b_5 ($cytb_5$) domain proteins, called $cytb_{5\underline{M}}$ (MAPR-like). Relative to classical $cytb_5$ proteins, MAPR and $ctyb_{5M}$ proteins shared unique sequence elements and a distinct heme-binding orientation at an approximately 90° rotation relative to classical $cytb_5$, as demonstrated in the archetypal crystal structure of a $cytb_{5M}$ protein (PDB accession number 6NZX). Here, we present the crystal structure of an archaeal $cytb_{5M}$ domain (*Methanococcoides burtonii* WP_011499504.1, PDB:6VZ6). It exhibits similar heme binding to the 6NZX $cytb_{5M}$, supporting the deduction that MAPR-like heme orientation was inherited from the prokaryotic ancestor of the original eukaryotic MAPR gene.

Keywords: cytochrome b5; membrane-associated progesterone receptor; steroidogenesis

We recently investigated a possible eukaryogenic role of MAPR proteins in early eukaryotic origins [1], prompted by the discovery that some mitochondrial genes had co-evolved with PGRMC1 [2], and that introducing point mutations at known phosphorylation sites on PGRMC1 had an effect on mitochondrial shape and mitochondrial protein abundance [3]. Several PGRMC1 functions also appear to be ancient in eukaryotes [1], including regulation of heme synthesis [4], cytP450 interactions [5] and sterol metabolism [2]. That investigation led to the discovery of the newly identified yet ancient $cytb_{5M}$ subclass of $cytb_5$-domain proteins, which were more similar to MAPR than to classical eukaryotic $cytb_5$ proteins and which therefore gave rise to MAPR proteins [1].

PGRMC1 is the archetypal and best characterised member of the heme-binding eukaryotic MAPR family [1,6] in which the heme-interacting tyrosine residue is

Abbreviations
CPR, candidate phyla radiation; $cytb_5$, cytochrome b_5; $cytb_{5M}$, MAPR-like cytochrome b_5; $cytb_{5MY}$, tyrosine-(Y)-containing $cytb_{5M}$ proteins; cytP450, cytochrome P450; FPLC, fast protein liquid chromatography; GST, glutathione S-transferase; MAPR, membrane-associated progesterone receptor (a eukaryotic family of cytochrome b5 domain proteins); MIHIR, MAPR-specific interhelical insertion region; NENF, Neudesin; NEUFC, Neuferricin; PDB, Protein Data Bank; PGRMC1, progesterone receptor membrane component 1; PGRMC2, progesterone receptor membrane component 2; RMSD, root-mean-square deviation; TEV, tobacco etch virus.

Y113, and residues Y107, K163 and Y164 hydrogen bond (H-bond) with heme [7]. A group of $cytb_{5M}$-like proteins from candidate phyla radiation (CPR) bacteria appear to exhibit similar tyrosinate heme chelation to MAPR proteins, because polar heme-interacting residues are strongly conserved with PGRMC1. We called these tyrosine-(Y)-containing $cytb_{5M}$-like proteins $cytb_{5MY}$. It has so far not been possible to determine whether MAPR proteins evolved from a CPR $cytb_{5MY}$, or whether $cytb_{5MY}$ arose after horizontal gene transfer of a MAPR gene into CPR bacteria [1].

In this study, we solved the crystal structure of a second $cytb_{5M}$ protein, which demonstrated substantial overall three-dimensional similarity to our previous $cytb_{5M}$ structure [1]. These results will contribute to our future characterisation of MAPR origins, and the understanding of how eukaryotes adapted ancient functions and invented novel ones to produce the first MAPR protein, whose strongly conserved inheritance into phylogenetically diverse eukaryotes suggests it performed essential roles in a very early eukaryote [1,6].

Methods

The archaeal *Methanococcoides burtonii* WP_011499504.1 protein selected for this study was previously identified as a $cytb_{5M}$ protein [1]. To produce pure protein to determine the structure by protein crystallisation, protein constructs were expressed and purified in *Escherichia coli PLysS* cells as previously described [1]. Briefly, the codon-optimised WP_011499504.1 open reading frame was subcloned into pGEX-4T-1-H expression vector (Genscript) to create pGEX4T1_WP011499504. Competent *E. coli BL21(DE3) PLysS* cells (Novagen, Darmstadt, Germany, #69451; 50 µL) were transformed with 1 µL of plasmid DNA using heat-shock method and cell recovery. Eighty microliter of cells were spread onto Luria base plates containing ampicillin (100 $\mu g \cdot mL^{-1}$) and incubated overnight at 37 °C. Luria broth containing ampicillin (100 $\mu g \cdot mL^{-1}$) was inoculated with the bacterial colonies and incubated overnight at room temperature at 220 r.p.m. MiniPrep (Qiagen, Aarhus, Denmark) was performed using the transformed *E. coli* cells as per the manufacturer's protocol. Large-scale cultures were produced using the transformed *E. coli* cells by adding 500 µL of cells to 500 mL of autoinduction expression base media containing 1% tryptone, 0.5% yeast extract, 1 mM $MgSO_4$, 5% 20× NPS (50 mM Na_2HPO_4, 50 mM KH_2PO_4 and 25 mM $(NH_4)_2SO_4$), 2% 50× 5052 (0.5% glycerol, 0.05% glucose and 0.2% lactose) and ampicillin (100 $\mu g \cdot mL^{-1}$). Cells were incubated at 30 °C at 80 r.p.m. for approximately 28 h. To perform glutathione S-transferase (GST) affinity chromatography using fast protein liquid chromatography (FPLC), the soluble cell extracts were injected using a superloop at 2 $mL \cdot min^{-1}$ into a GST column equilibrated with GST cell lysis buffer. The column was washed with 10 column volumes of GST buffer (50 mM Tris(hydroxymethyl)aminomethane, 125 mM NaCl, pH 7.4). Competitive binding using GST buffer containing 10 mM glutathione eluted purified GST-tagged protein from the column. To cleave the N-terminal GST tag from the protein, 100 µL of tobacco etch virus (TEV) protease was added to the protein eluate and incubated at 4 °C overnight with TEV. Size exclusion chromatography was performed using AKTA FPLC with S200 20/60 filtration column equilibrated with 50 mM Tris. The purity of the samples and the complete cleavage of the $cytb_{5M}$ domain from the affinity tag were assessed using SDS/PAGE analysis.

Diffractable protein crystals were produced in an optimised condition from the PEG ION 2 screen (Hampton Research) using purified protein at 8 $mg \cdot mL^{-1}$ in a condition containing 0.1 M succinic acid, 12% PEG6000 incubated at 23 °C. Crystals produced from a crystal optimisation were flash frozen using liquid nitrogen in a 20% glycerol stock and sent for x-ray diffraction to the Australian Synchrotron Facility, Melbourne. Crystal data were collected using the MX2 (Eiger 16 M detector) crystal beamline [8,9] and BLU-ICE software [10] at the Australian Synchrotron Facility. The data were integrated in IMOSFLM [11] scaled and reduced in AIMLESS [12]. The structure was determined by molecular replacement using PDB ID 1J03 in PHASER [13], REFMAC [14], PHENIX [15] and COOT [16].

Sedimentation velocity experiments were performed at 25 °C in a Beckman Coulter XL-A analytical ultracentrifuge as previously described [17]. Double-sector cells containing synthetic quartz windows were loaded with 380 µL of protein at 1 $mg \cdot mL^{-1}$ and 400 µL of 50 mM Tris as a reference. Cells were centrifuged at 100 000 ***g*** using a 4-hole An-50 Ti rotor while data were collected in continuous mode without averaging at 280 nm with a radial step size of 0.003 cm. Solvent density (0.9997 $g \cdot mL^{-1}$), solvent viscosity (0.01017 cp) and estimated protein partial specific volume (0.7386 $mL \cdot g^{-1}$) were computed using SEDNTERP [18]. SEDFIT was used to fit absorbance as a function of radial position to the Lamm equation to determine the continuous sedimentation and mass coefficient distributions [18,19].

Results

Methanococcoides burtonii WP_011499504.1 $cytb_{5M}$ protein purification

Both the *M. burtonii* $cytb_{5M}$ protein and our previously described *Hadesarchaea* $cytb_{5M}$ protein structure (PDB: 6NZX) [1] are from the archaeal Euryarchaeota taxon. The archaeal *M. burtonii* $cytb_{5M}$ domain was recombinantly expressed and purified (Fig. 1A–C)

prior to successful crystallisation and structural comparisons with the crystal structure of the $cytb_5$ domains of PGRMC1 (PDB: 4X8Y) [7] and the *Hadesarchaea* $cytb_{5M}$ protein structure (PDB: 6NZX) [1]. The *M. burtonii* $cytb_{5M}$ domain existed predominantly as an ~ 8 kDa monomer in solution on S200 gel filtration profile (Fig. 1B), and a peak at ~ 50 kDa is also present on the gel filtration profile, representing a dimer of the GST affinity tag (Fig. 1B). The results were confirmed in analytical ultracentrifugation experiments, which resulted in peaks spanning sedimentation coefficient ranges of 0.4–2 S and 3.2–4.5 S. These values are consistent with species of ~ 8 kDa and ~ 50 kDa, respectively, based on c(*M*) analyses (Fig. 1D,E).

Crystal structure of the *Methanococcoides burtonii* WP_011499504.1 $cytb_{5M}$ domain

Protein crystals were produced in an optimised condition from the PEG ION 2 screen (Hampton Research) using purified *M. burtonii* $cytb_{5M}$ domain protein at 8 $mg{\cdot}mL^{-1}$ in a condition containing 0.1 M succinic acid, 12% PEG6000 incubated at 23 °C (Fig. 2A). The structure of the *M. burtonii* $cytb_{5M}$ domain was solved to a resolution of 2.1 Å (Table 1) and contained a well-ordered heme molecule in the cofactor binding site (Fig. 2B). This is consistent with the red coloration of the protein in solution and of the protein crystals (Fig. 2A) and was also evidenced through absorbance at ~ 412 nm using spectroscopy (not shown). Although the heme is not covalently bonded in the structure of the *M. burtonii* $cytb_{5M}$ domain, it is buried within the protein (Fig. 2C).

Diffraction data were indexed and integrated in the space group P 41 2 2, with unit cell dimensions of a = 67.495=, b = 67.495 and c = 48.132, and angles of a = 90, b = 90 and c = 90. Following rebuilding and refinement in COOT and REFMAC, respectively, the final model had an *Rwork* and *Rfree* of 0.1622 and 0.1953, respectively, no Ramachandran outliers, and good stereochemistry (Table 1). The structure was analysed using Proteins, Interfaces, Structures and Assemblies (PISA) [20]. The protein and heme ligand complex had an interface area of 524.4 Å (Fig. 2C). The coordinates and associated structural data were deposited and validated to the Protein Data Bank (PDB) and issued the code 6VZ6.

As predicted from the protein sequences, there is high structural similarity between the *M. burtonii* and the *H. archaeon ynp_n21* $cytb_{5M}$ domains (Fig. 3A). The main polar interactions with heme include the side chains of S34, H42 and H61 (Fig. 3B). The H-bond interactions are shown in Fig. 3E. The structure of *H. archaeon ynp_n21* $cytb_{5M}$ domain showed heme chelation through residues H42 and H61 (Fig. 3C). The cognate residues were involved in H-bonding in *M. burtonii* $cytb_{5M}$ domain (Fig. 3B). Differences in the residues that interact with heme between $cytb_{5M}$ and MAPR proteins indicate the appearance of novel heme-binding properties in the evolutionary transition from prokaryotic $cytb_{5M}$ to eukaryotic MAPR proteins, as exemplified by PGRMC1 (4X8Y [7]; Fig. 3D,G).

A heuristic PDB search was performed using DALI protein structure comparison by alignment of distance matrices [21] to identify the protein structures, from those available on the PDB, with the highest structural homology to the *M. burtonii* $cytb_{5M}$ domain (Table 2). As expected, the *M. burtonii* $cytb_{5M}$ domain showed highest homology to the *H. archaeon ynp_n21* $cytb_{5M}$ domain with a root-mean-square deviation (RMSD) of 0.7 and %ID of 54%. The protein identified with the second highest confidence score was the PGRMC1 $cytb_5$/MAPR domain, although comparatively, the similarity was much lower, with an RMSD of 2.2 and %ID of 23%. All other identified sequences belong to the classical type $cytb_5$ group, underlining the novelty of the $cytb_{5MY}$ structural fold and its similarity to the only solved MAPR crystal structure, that of PGRMC1.

Discussion

MAPR proteins originated from a prokaryotic $cytb_{5M}$ domain protein, or possibly from the subclass $cytb_{5MY}$, rather than from the conventionally recognised $cytb_5$ proteins that gave rise to classical mammalian $cytb_5$ proteins [1]. Here, we present the second structure of a $cytb_{5M}$ protein, from *M. burtonii* (WP_011499504.1). Unlike PGRMC1, the heme iron atom of both the archaeal *H. archaeon ynp_n21* and *M. burtonii* WP_011499504.1 $cytb_{5M}$ domains are coordinated by two conserved histidine residues that serve as axial ligands (H42 and H61). The dual histidine mode of heme chelation (Fig. 3) is conserved in $cytb_{5M}$ domain proteins such as the previous 6NZX $cytb_{5M}$ structure, as well as classical $cytb_5$ domain-containing proteins [1]. The heme is buried within the cleft, further supported through conserved H-bonding at S34. This differs from the tyrosinate Y113-mediated heme Fe chelation observed in PGRMC1 [7]. The situation in other MAPR proteins remains unknown but is presumed to resemble PGRMC1. Differences in heme binding are attributable to evolutionary modification of heme-interacting residues in PGRMC1 relative to the $cytb_{5M}$ proteins (Figs 3 and 4).

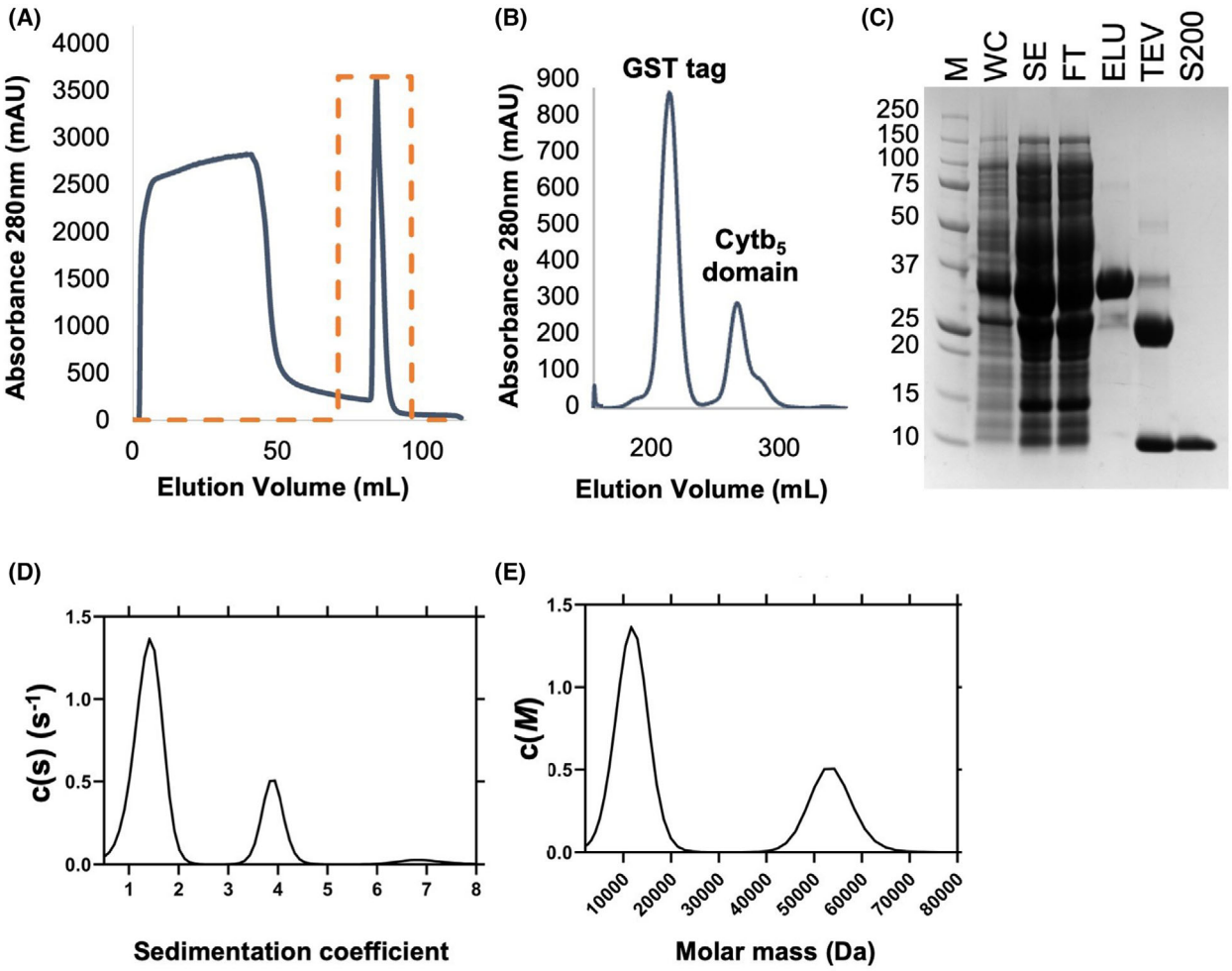

Fig. 1. *Methanococcoides burtonii* WP_011499504.1 $cytb_{5M}$ domain expression and purification. (A) GST affinity purification of the *M. burtonii* $cytb_{5M}$ domain UV trace (blue) and fractions containing purified protein (purple). (B) S200 size exclusion chromatography of the $cytb_{5M}$ domain. (C) SDS/PAGE analysis showing a purified protein band at ~ 8 kDa. M, marker; WC, whole-cell extract; SE, soluble extract; FT, flow through; GST, GST-tagged purified protein (~ 33 kDa); TEV, cleavage of GST tag (~ 25 kDa) with TEV protease from purified protein (~ 8 kDa); S200, purified protein (~ 8 kDa). (D) The continuous sedimentation coefficient distribution and (E) the continuous mass coefficient distribution resulting from sedimentation velocity analysis of the *M. burtonii* $cytb_{5M}$ domain at a concentration of 1 mg·mL^{-1} by analytical ultracentrifugation. Continuous sedimentation coefficient distribution analysis resulted in peaks at ~ 1.5 S and ~ 4 S, which are consistent with the $cytb_{5M}$ monomer and GST-tag dimer, respectively, as determined by the continuous mass coefficient distribution.

While the prokaryotic $cytb_{5M}$ and $cytb_{5MY}$ proteins share a conserved surface patch and heme-binding pocket similarities with MAPR proteins, they lack a MAPR-specific interhelical insertion region (MIHIR) sequence that is found in MAPR proteins. The PGRMC1 MIHIR extends from L130 to E157 in the protein sequence (Fig. 4), between residues that H-bond with heme, but which loop away to the opposite protein surface from the heme-binding site in the folded protein structure [1,7]. A conserved motif in the MIHIR region of PGRMC1 resembles a coiled-coil motif found in several myosin proteins, suggesting that PGRMC1 may interact with some of the same proteins as myosins, that is components of the actin cytoskeleton [6]. PGRMC1 was co-immunoprecipitated with actin cytoskeleton-associated proteins including RACK1 and α-Actinin-1 [22,23]. Therefore, the MIHIR, a eukaryotic invention, may be involved with actin cytoskeletal interactions. Point mutations at known phosphorylation sites on PGRMC1 including tyrosine residue 180 affected cell motility and altered the protein abundance of actin cytoskeleton-associated proteins [3,24]. It is probable that interactions between PGRMC1 and components of the actin cytoskeleton, predicted to occur within the

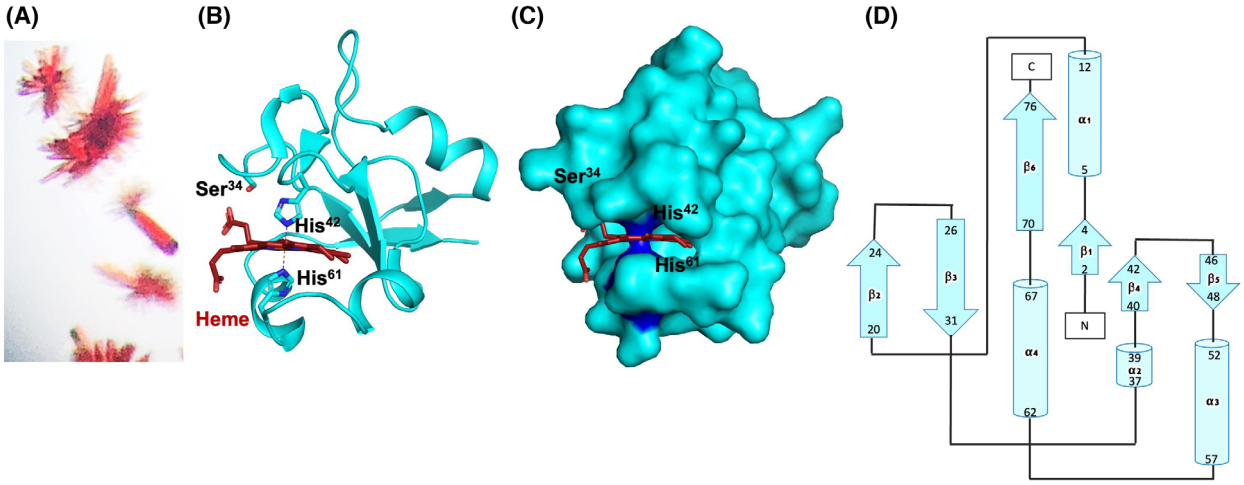

Fig. 2. Schematic representation of the structure of the *Methanococcoides burtonii* WP_011499504.1 $cytb_{5M}$ domain. (A) Crystals were obtained in 0.1 M succinic acid, 12% PEG6000 at 23 °C. The red coloration is due to the presence of the heme ligand. (B) The structure of the $cytb_{5M}$ domain (blue) showing a heme-bound ligand (red). (C) Surface representation (blue) and the heme ligand (red), which is buried within the $cytb_{5M}$ domain. Key interacting residues (S3, H42 and H61) are shown. (D) Topology map obtained from PDBsum showing alpha helices (cylindrical) and beta sheets.

Table 1. Crystallography data collection and refinement statistics. Statistics for the highest-resolution shell are shown in parentheses.

Resolution range	67.5–2.1
Space group	P 41 2 2
Unit cell	67.495 67.495 48.132 90 90 90
Reflections	6908
Multiplicity	7.1 (4.8)
Completeness (%)	98.0 (95.0)
Mean I/sigma(I)	14.3 (5.1)
R-merge	0.089 (0.297)
R-meas	0.096 (0.334)
R-pim	0.033 (0.149)
CC1/2	0.997 (0.946)
Reflections used in refinement	6717 (631)
R-work	0.1622
R-free	0.1953
Number of nonhydrogen atoms	726
Macromolecules	617
Ligands	43
Solvent	66
Protein residues	79
RMS (bonds)	0.0102
RMS (angles)	1.04
Ramachandran favoured (%)	98.67
Ramachandran allowed (%)	1.33
Ramachandran outliers (%)	0.00
Rotamer outliers (%)	0.00
Clashscore	4.84
Average B-factor	24.8
Macromolecules	24.2
Ligands	22.1
Solvent	32.7

previously described MIHIR sequence, could be regulated by tyrosine phosphorylation [6].

Neither of the archaeal $cytb_{5M}$ proteins exhibited a heme-dependent dimerization, as reported for PGRMC1 [7]. We note heme-stacking interactions observed in the PGRMC1 crystal structure could also potentially facilitate even larger multimer formation. This merits future investigation. PGRMC1 dimers or higher-order structures have been observed not only in the bacterially expressed crystallised protein [7], but also in mammalian cells [25], where an anti-FLAG tag antibody can immunoprecipitate FLAG-tagged as well as endogenous PGRMC1. Endogenous PGRMC1 precipitation was dependent upon heme availability. Also, the molecule glycyrrhizin (the active compound in liquorice), and derivatives, binds to PGRMC1 residues involved in the dimeric interface, disrupting the protein complex and favouring monomer formation [25].

Although the structure of a $cytb_{5MY}$ protein could be informative, we have so far been unable to obtain one. Future determination of the structures of other MAPR proteins and $cytb_{5MY}$ proteins will be required to determine whether tyrosinate heme chelation is commonly accompanied by heme-mediated dimerisation. The shared $cytb_{5M}$/MAPR orientation of heme binding is presumably related to an important MAPR-dependent eukaryotic function. In light of the current understanding of the structural differences between MAPR proteins, $cytb_{5M}$ and classical $cytb_5$ proteins,

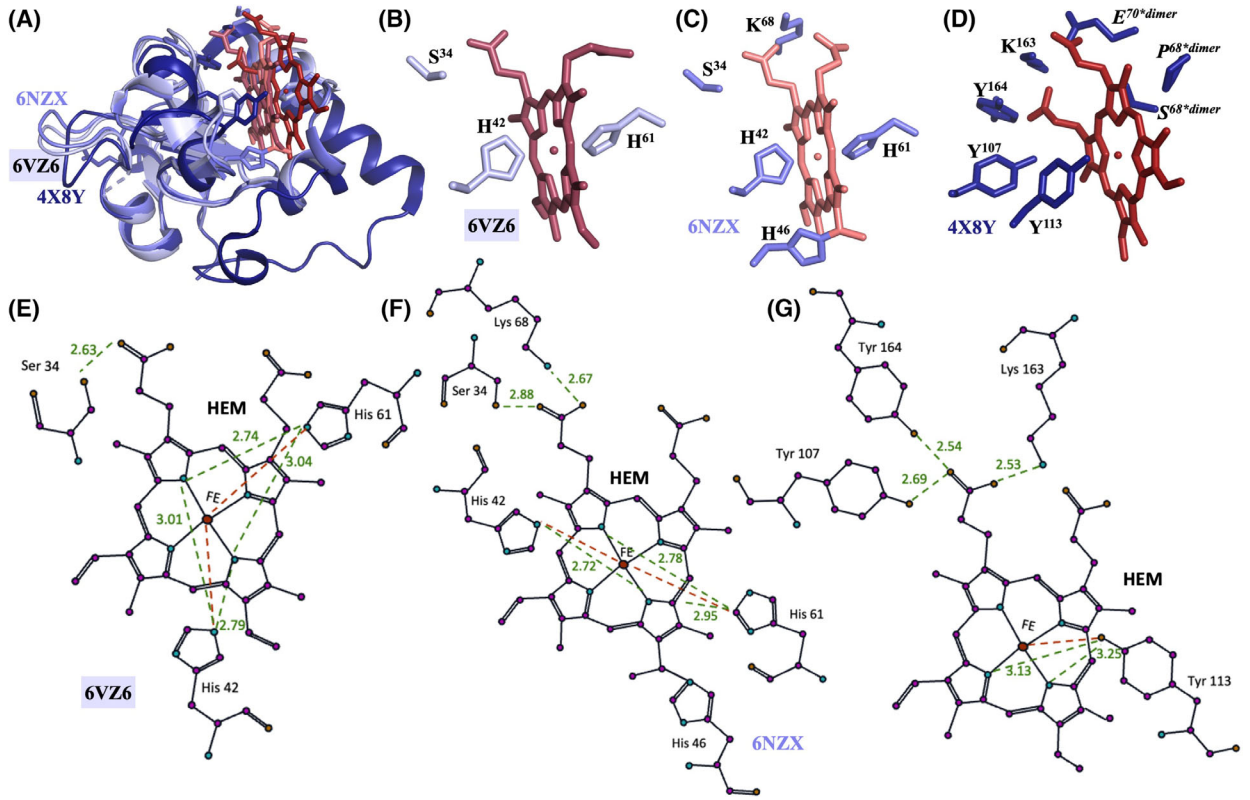

Fig. 3. Heme axial binding within the cytb$_{5M}$ domain. (A) Overlay of archaeal cytb$_{5M}$ domains and PGRMC1 cytb$_5$/MAPR domain structures from PDB. The PGRMC1 cytb$_5$ domain has a longer helix than the *H. archaeon ynp_n2* and *M. burtonii* cytb$_{5M}$ domains, which is shifted away from the heme molecule. (B) Heme binding within the *M. burtonii* WP_011499504.1 cytb$_{5M}$ domain involves H-bonding at S34 and heme Fe axial ligand support at H42 and H61. (C) Heme binding within the *H. archaeon ynp_n21* cytb$_{5M}$ domain involves binding at H46, H-bonding at S34 and K68 residues and heme axial ligand support at H42 and H61. (D) Heme binding within the PGRMC1 cytb$_5$/MAPR domain is coordinated through Y113 residue and H-bonding at Y107, K163 and Y164. Note the absence of Fe-interacting axial histidine residues, indicating that this type of heme interaction differs from that seen for the archaeal cytb$_{5M}$ proteins. (E–G) are adapted from figures produced using LIGPLOT [28]. Note the residues in orange (S68, P69 and E70) are interactions from the bacterial expression vector with the heme, not PGRMC1 residues, as previously discussed [1]. (E) Heme binding in the *M. burtonii* WP_011499504.1 cytb$_{5M}$ domain. (F) Heme binding in the *H. archaeon ynp_n21* cytb$_{5M}$ domain. (G) Heme binding within the cytb$_5$/MAPR domain of PGRMC1.

Table 2. Structural comparison of proteins with the highest structural homology to archaeal *Methanococcoides burtonii* cytb$_{5M}$ domain with the structure of 6VZ6. %ID, per cent identity; LALI, total number of aligned residues; Nres, total number of residues; RMSD, root-mean-square deviation across the aligned sequences; Z, z-score confidence in similarity significance.

PDB ID	z	RMSD	LALI	Nres	%ID	Protein name	Gene	Organism
6NZX	16.4	0.7	76	76	54	Cytochrome b5	APU95_03975	*H. archaeon YNP_N21*
4X8Y	8.3	2.2	73	112	23	Progesterone receptor membrane component 1	PGRMC1	*Homo sapiens*
1SOX	8.2	2.0	69	463	25	Sulfite oxidase	SUOX	*Gallus gallus*
1X3X	8.0	2.4	71	82	25	Cytochrome b5	N/A	*Ascaris suum*
1KBI	5.9	2.4	67	504	30	Cytochrome b2	CYB2	*Saccharomyces cerevisiae*
2I96	5.8	2.8	69	108	25	Cytochrome b5	CyB5A	*Homo sapiens*
2KEO	2.6	3.6	46	92	28	Probable E3 ubiquitin-protein ligase HERC2	HERC2	*Homo sapiens*

```
6VZ6 --MEEFTTEELAKYNGKDGEKCYFAYKGKVYDVTESML-WEDGDHQGMHEGGIDLTADHEDAPHD  62
                          Δ          o Δ-Δ    xΔ ΔΔ     Δ  ΔΔ  ΔΔx
6NZX --MRVFTKEELSRYNGKEGAPAYVAYNGKVYDVTGSFH-WKGGKHHVLHDAGQDLTESIGRAPHT  62
                                     o Δ-Δ    xΔ  o     Δ  ΔΔ ΔΔΔx
4X8Y SPEFDFTPAELRRFDGVQDPRILMAINGKVFDVTKGRKFYGPEGPYG-VFAGRDASRGLATFCLD 131
     ▲▲▲                                 Δo     x           ΔΔ ΔΔΔ
    *LKRR                                                          MIHIR

6VZ6 -------------------------DD-VLEDFPVVGTLKA-----------------------  77
                               ΔΔ Δ
6NZX -------------------------AE-LLEKFPVVGVLRD-----------------------  77
                               ΔΔoΔ
4X8Y KEALKDEYDDLSDLTAAQQETLSDWESQFTFKYHHVGKLLKEGEEPTVYSDEEEPKDESARKND 195
                          Δ   ΔΔ oo
                MIHIR
Heme interactions
Δ hydrophobic interactions; o H-bonds; x axial ligation
```

Fig. 4. Sequence alignment of *M. burtonii* (6VZ6) and *H. archaeon ynp_n21* (6NZX) $cytb_{5M}$ domains and PGRMC1 (4X8Y) $cytb_5$ domain from a structural comparison using the *M. burtonii* $cytb_{5M}$ domain protein sequence (6VZ6) as the reference. Residues conserved in all three proteins are highlighted in grey. Filled triangles (▲) at the N-terminus of 4X8Y represent heme interactions with non-PGRMC1 residues in 4X8Y that are contributed by the bacterial protein expression cloning vector (boxed). The asterisked PGRMC1 residues 67–71 show the wild-type PGRMC1 sequence. Numbering refers to PGRMC1 (O00264) residues. The gapped alignment of the top (6VZ6 1–62) is based on the alignment of 1620 cytb5 domain proteins of clades-1 and -2 from Tamarit et al. ([1], Fig. 3A), as is the position off the MAPR-specific interhelical insertion region (MIHIR) of PGRMC1. The lower alignment (6VZ6 63–77) is generated here based upon heme interactions.

including MAPR tyrosinate coordinated heme binding, heme orientation, and the presence and function of the MIHIR binding region, future research should investigate the origins and function of MAPR proteins, with particular focus on the PGRMC1 membrane trafficking function [26,27].

Acknowledgements

This research was supported by Charles Sturt University School of Biomedical Sciences (MAC), an APA PhD scholarship (ST), an Australian Government Research Training Program Scholarship (ERRM) and a Grains Research and Development Corporation (9176977) PhD scholarship (ERRM) and operational funding (JKF, ERRM). This research was partly undertaken on the macromolecular crystallography beamlines at the Australian Synchrotron, part of ANSTO (DA). TPSC would like to thank the Australian Research Council (DE190100806) for fellowship and funding support. We also thank the La Trobe University Comprehensive Proteomics Platform for providing infrastructure support. Open access publishing facilitated by Charles Sturt University, as part of the Wiley - Charles Sturt University agreement via the Council of Australian University Librarians. Open access publishing facilitated by Charles Sturt University, as part of the Wiley - Charles Sturt University agreement via the Council of Australian University Librarians.

Author contributions

Conceptualization (MAC), designed and performed experiments (ST, MM, ST and ERRM), x-ray diffraction and data collection (DA), data analysis (JKF, ST, ERRM and TPSC), manuscript preparation (ST and MAC) and manuscript revision (JKF, ERRM and TPSC).

Additional information

This research was undertaken in part using the MX2 beamline at the Australian Synchrotron, part of ANSTO, and made use of the Australian Cancer Research Foundation (ACRF) detector. The Full wwPDB X-ray Structure Validation Report for the resulting structure is provided as Appendix S1.

Data accessibility

Data to support the findings of this study are openly available in the Protein Data Bank at https://www.rcsb.org/, reference number 6VZ6.

References

1 Tamarit D, Teakel S, Marama M, Aragao D, Gerdes SY, Forwood JK, et al. MAPR origins reveal a new class of prokaryotic cytochrome b5 proteins and possible role in eukaryogenesis. *BioRxiv*. 2021. https://doi.org/10.1101/2021.11.17.468889

2 Cahill MA, Medlock AE. Thoughts on interactions between PGRMC1 and diverse attested and potential hydrophobic ligands. *J Steroid Biochem Mol Biol*. 2017;**171**:11–33.

3 Thejer BM, Adhikary PP, Kaur A, Teakel SL, Van Oosterum A, Seth I, et al. PGRMC1 phosphorylation affects cell shape, motility, glycolysis, mitochondrial form and function, and tumor growth. *BMC Mol Cell Biol*. 2020;**21**:24.

4 Piel RB 3rd, Shiferaw MT, Vashisht AA, Marcero JR, Praissman JL, Phillips JD, et al. A novel role for progesterone receptor membrane component 1 (PGRMC1): a partner and regulator of Ferrochelatase. *Biochemistry*. 2016;**55**:5204–17.

5 Ryu CS, Klein K, Zanger UM. Membrane associated progesterone receptors: promiscuous proteins with pleiotropic functions – focus on interactions with cytochromes P450. *Front Pharmacol*. 2017;**8**:159.

6 Hehenberger E, Eitel M, Fortunato SAV, Miller DJ, Keeling PJ, Cahill MA. Early eukaryotic origins and metazoan elaboration of MAPR family proteins. *Mol Phylogenet Evol*. 2020;**148**:106814.

7 Kabe Y, Nakane T, Koike I, Yamamoto T, Sugiura Y, Harada E, et al. Haem-dependent dimerization of PGRMC1/Sigma-2 receptor facilitates cancer proliferation and chemoresistance. *Nat Commun*. 2016;**7**:1–13.

8 Aragão D, Aishima J, Cherukuvada H, Clarken R, Clift M, Cowieson NP, et al. MX2: a high-flux undulator microfocus beamline serving both the chemical and macromolecular crystallography communities at the Australian Synchrotron. *J Synchrotron Radiat*. 2018;**25**:885–91.

9 Cowieson NP, Aragao D, Clift M, Ericsson DJ, Gee C, Harrop SJ, et al. MX1: a bending-magnet crystallography beamline serving both chemical and macromolecular crystallography communities at the Australian Synchrotron. *J Synchrotron Radiat*. 2015;**22**:187–90.

10 McPhillips TM, McPhillips SE, Chiu HJ, Cohen AE, Deacon AM, Ellis PJ, et al. Blu-ice and the distributed control system: software for data acquisition and instrument control at macromolecular crystallography beamlines. *J Synchrotron Radiat*. 2002;**9**:401–6.

11 Battye TG, Kontogiannis L, Johnson O, Powell HR, Leslie AG. iMOSFLM: a new graphical interface for diffraction-image processing with MOSFLM. *Acta Crystallogr D Biol Crystallogr*. 2011;**67**:271–81.

12 Evans PR, Murshudov GN. How good are my data and what is the resolution? *Acta Crystallogr D Biol Crystallogr*. 2013;**69**:1204–14.

13 McCoy AJ. Solving structures of protein complexes by molecular replacement with phaser. *Acta Crystallogr D Biol Crystallogr*. 2007;**63**:32–41.

14 Murshudov GN, Vagin AA, Dodson EJ. Refinement of macromolecular structures by the maximum-likelihood method. *Acta Crystallogr D Biol Crystallogr*. 1997;**53**:240–55.

15 Adams PD, Afonine PV, Bunkóczi G, Chen VB, Davis IW, Echols N, et al. PHENIX: a comprehensive python-based system for macromolecular structure solution. *Acta Crystallogr D Biol Crystallogr*. 2010;**66**:213–21.

16 Emsley P, Lohkamp B, Scott WG, Cowtan K. Features and development of Coot. *Acta Crystallogr D Biol Crystallogr*. 2010;**66**:486–501.

17 Soares da Costa TP, Patel M, Desbois S, Gupta R, Faou P, Perugini MA. Identification of a dimeric KDG aldolase from agrobacterium tumefaciens. *Proteins*. 2017;**85**:2058–65.

18 Laue T. Biophysical studies by ultracentrifugation. *Curr Opin Struct Biol*. 2001;**11**:579–83.

19 Schuck P, Perugini MA, Gonzales NR, Howlett GJ, Schubert D. Size-distribution analysis of proteins by analytical ultracentrifugation: strategies and application to model systems. *Biophys J*. 2002;**82**:1096–111.

20 Krissinel E, Henrick K. Inference of macromolecular assemblies from crystalline state. *J Mol Biol*. 2007;**372**:774–97.

21 Holm L. Benchmarking fold detection by DaliLite v.5. *Bioinformatics*. 2019;**35**:5326–7.

22 Teakel SL, Ludescher M, Thejer BM, Poschmann G, Forwood JK, Neubauer H, et al. Protein complexes including PGRMC1 and Actin-associated proteins are disrupted by AG-205. *Biochem Biophys Res Commun*. 2020;**524**:64–9.

23 Salsano S, Gonzalez-Martin R, Quinonero A, Lopez-Martin S, Gomez-Escribano AP, Perez-Deben S, et al. Novel nonclassic progesterone receptor PGRMC1 pulldown-precipitated proteins reveal a key role during human decidualization. *Fertil Steril*. 2020;**113**:1050–66.e7.

24 Thejer BM, Adhikary PP, Teakel SL, Fang J, Weston PA, Gurusinghe S, et al. PGRMC1 effects on metabolism, genomic mutation and CpG methylation imply crucial roles in animal biology and disease. *BMC Mol Cell Biol*. 2020;**21**:26.

25 Kabe Y, Koike I, Yamamoto T, Hirai M, Kanai A, Furuhata R, et al. Glycyrrhizin derivatives suppress cancer chemoresistance by inhibiting progesterone receptor membrane component 1. *Cancer*. 2021;**13**:3265.

26 Cahill MA, Jazayeri JA, Catalano SM, Toyokuni S, Kovacevic Z, Richardson DR. The emerging role of progesterone receptor membrane component 1 (PGRMC1) in cancer biology. *Biochim Biophys Acta*. 2016a;**1866**:339–49.
27 Hampton KK, Stewart R, Napier D, Claudio PP, Craven RJ. PGRMC1 elevation in multiple cancers and essential role in stem cell survival. *Adv Lung Cancer (Irvine)*. 2015;**4**:37–51.
28 Wallace AC, Laskowski RA, Thornton JM. LIGPLOT: a program to generate schematic diagrams of protein-ligand interactions. *Protein Eng*. 1995;**8**: 127–34.

Supporting information

Additional supporting information may be found online in the Supporting Information section at the end of the article.

Appendix S1 Full wwPDB X-ray Structure Validation Report.